

Numerical Analyses of Loaded Strip Footing Resting on Cellular Mattress and Strips: Reinforced Fly Ash Slope

Maheboobsab B. Nadaf¹ · J. N. Mandal¹

Received: 3 July 2017 / Accepted: 9 August 2017 / Published online: 16 August 2017
© Springer International Publishing AG 2017

Abstract In this paper, unreinforced and cellular reinforced fly ash slopes were analyzed using numerical modelling to simulate the laboratory model studies by applying similar geometry and reinforcement parameters to understand its deformation behavior on rigid foundation. Small scale laboratory experimental models were performed on fly ash slopes by applying strip loading at a 60° inclination. In the current study an approach was made to use cellular reinforcement (CR) material which is made up of from post-consumer waste plastic water bottles along with steel grid-jute geotextile composite reinforcement at slope facia. A numerical analyses using finite-element analysis (FEA) PLAXIS 3D was conducted to validate the experimental laboratory model test results. In FEA, fly ash as backfill material and reinforcing materials like steel grid-jute geotextile and cellular/geocell reinforcement were modeled systematically. Here, fly ash modeled with Mohr–Coulomb failure criteria as linear elastic plastic material and, for cellular/geocell reinforcement it was modeled as elastoplastic material. The numerical model analyses were consistently substantiated with experimental results. Parametric analysis were conducted by using validated numerical model to evaluate the influence of various cellular properties along with steel grid-jute geotextile composite reinforcement on the performance of reinforced fly ash slopes. The numerical finite element simulation (FES) results are in good agreement with the model test results.

Keywords Fly ash · Slope · Cellular reinforcement · Rigid foundation · Strip loading · Finite-element analysis

Introduction

Fly ash is produced by burning coal from thermal power plants (TPPs) and it has become major source to generate power in India. According to Kumar et al. [1] fly ash production is expected to reach 225 Mt by 2017 due to rising demand for power whereas; use of fly ash is only 45 Mt per year. In India, huge quantity of natural materials like soils, sand and aggregates are being utilized as structural filling material as well as constructional material. It has created severe scarcity of these conventional materials in their specific uses, cultivation and ecology ecosystems. In India, with enhancing demand of power, generation of fly ash from TPPs is anticipated to reach 225 million tonne by the year 2017 [2], and 90×10^6 tonnes per year demanding an area of 265 km² pond ash [3], and few years back, only <5% of this fly ash was usefully utilized. The disposal of fly ash and other Pozzolanic materials like wastes coming out of TPPs and other industrial units has been the major concern worldwide over the decades due to scarcity of the land available for their disposal. Civil engineers are forced to make use of unsuitable sites mainly low lying regions after filling them by means of fly ash which is waste byproduct material due to decreasing availability of good construction sites and increasing constructional activities. Moreover, in the developing country like India this problem is more acute. Utilization of fly ash as a filling material is one of the promising areas in structural fills or embankments, whereby the construction cost of the projects can be reduced. In addition to this, it will encourage the sustainable development and reduce the environmental problems.

✉ Maheboobsab B. Nadaf
maheboob_nadaf@iitb.ac.in

J. N. Mandal
cejnm@civil.iitb.ac.in

¹ Civil Engineering Department, Indian Institute of Technology Bombay, Powai, Mumbai 400 076, India

Structural fly ash embankments are not uncommon but often are perceived as demonstration projects [4]. During last two decades, researchers extensively reported on the use of geosynthetic (polymeric) reinforcement as horizontal sheets in fly ash as a backfill material provides viable solution in enhancement of load bearing capacity of foundation soils like embankments, slopes, retaining walls etc., and if this is found effective, fly ash can be used in bulk quantity mainly for rail and road embankments in geotechnical applications. Preceding to prototype use, it is essential to conduct experimental and numerical methods in order to know the role of reinforcement materials in enhancing footing behaviour located near to the crest of fly ash slope. Several studies have been reported on stabilised sand slopes to know behaviour of footings [5–9]. However, only limited studies are available in the literature [10–12] on load-carrying capacity of footing behaviour resting on reinforced fly ash. Recently, Nadaf and Mandal [13] reported experimental studies conducted on fly ash slope reinforced with planar steel grid material in the form of continuous mattress and strips to know load bearing capacity of slope. Numerical design practices like FEA and finite-difference (FD) become prominent in recent years, but despite of many studies [14–19], much studies on footing resting on reinforced fly ash slopes remains to be carried out for safe and economical design. Extensive investigations were carried by several researchers on fly ash as a fill material [20–29]. Few researchers, Indraratna et al. [30] and Lim and Chu [31] worked on other Pozzolanic materials with reference to the bearing capacity behavior of footings.

Although much work has been done on the retaining walls and bearing capacity of the reinforced earth sub-grades throughout the world, work on bearing capacity of footings located on the apex of reinforced earth slopes or on the face of a slopes are still quite meager and only few works are available [32–43]. Most of the works used geogrid as the reinforcement; few used geocells [44, 45] and grid-anchors as the reinforcements. Relatively very less work is carried out in contest of reinforced fly ash slopes or embankments of other Pozzolanic materials. In recent past experimental, theoretical and numerical analysis on the bearing capacity of strip footing on reinforced fly ash slopes are reported [46, 47]. While majority of works entailed experimental work, some of them also attempted numerical analysis using FEA to compare the experimental results with those obtained numerically. The geocell mattresses are generally filled with granular geomaterial. The growing industrial activities create a huge amount of unwanted materials or byproducts that cannot be assimilated in the environment and end up being dumped as waste material. Even if the waste material is nonhazardous, it contributes to land scarcity. The best way to deal with this sort of challenge is to reuse those waste

materials in an effective sustainable fashion in a real-life application. Even the disposal of fly ash waste and waste plastic bottles also poses the environmental problem.

On the backdrop, relatively less work reported in the literature pertaining to strength evaluation and performance studies of the embankments made up of Pozzolanic materials either unreinforced or reinforced with respect to loaded footing. The present investigation was undertaken to study the bearing capacity behavior of unreinforced and cellular reinforced fly ash embankments with respect to numerical analysis was carried out by finite element based software 'PLAXIS 3D' in the contest by varying edge distance from slope crest to the top of footing plate. Cellular reinforcements were made up of post-consumer plastic water bottles along with steel grid-jute geotextile composite reinforcement was considered in this analysis. A 50 mm diameter of cellular reinforcement with variable geocell heights of 10, 20 and, 30 mm and edge distance (D_e) was varied as $1.0B$, $1.5B$, and $2.0B$ (B = Footing width) from slope crest was used in model tank tests. The three-dimensional reinforcement layers were positioned keeping an even vertical spacing (S_r) of $0.2H$ (H = Height of slope), while reinforcements were in strip forms with coverage ratios of 0.5 and 0.6 and in continuous form, i.e., coverage ratio (C_r) of 1. Coverage ratio is defined as the ratio of gross width of the reinforcement (b_h) to the center-to-center horizontal spacing between the strips (S_h), i.e. ($C_r = b_h/S_h$) [48]. Length of cellular reinforcement (L_r) was varied from 0.7 to 0.3 times the height of slope for both continuous form (mattress) and coverage ratios in the form of strips. The results of footing pressure (P)—footing settlement (S) responses of the slopes emerging out of the numerical analysis is in good agreement with those observed in the experimental studies, and are quite encouraging and can be used in the prototype constructions after taking certain precautions. The results of the numerical studies though agree well with those observed in the experimental studies [49], and are on lower side as compared to that obtained experimentally. It is obvious because the field conditions cannot be simulated that exactly in the numerical analysis.

Validation of Numerical Simulation Program

In the laboratory, small-scale model tests were performed on fly ash slopes with unreinforced and reinforced cellular mattress and strips under strip loading in a model tank with the dimensions of 1000 mm length \times 500 mm width \times 750 mm height [49]. Figure 1a, b show the schematic and laboratory model test setup. The strained controlled test was performed by placing a rigid steel plate of 10 mm thick, length 500 mm and width 100 mm at varying edge distances on top of slope being pushed vertically downward by means of a hydraulic jack at constant rate of 2 mm/min. The numerical

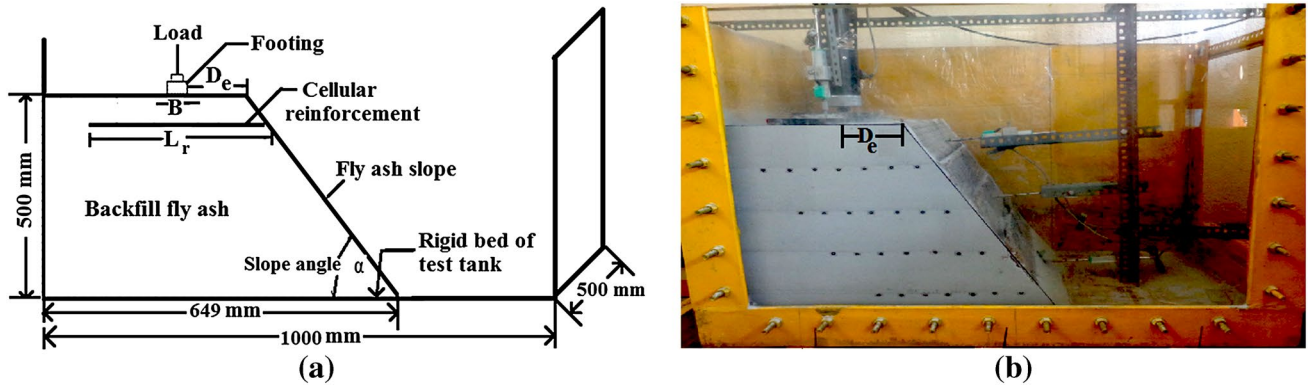


Fig. 1 a Schematic of the test setup; b small-scale model test setup

Table 1 Numerical finite-element simulation (FES) program for fly ash slopes on rigid foundation

Models	Cellular reinforcement (CR)	
	Dimensions	Parameters
Model-1: unreinforced (UR) test	–	Constant: $B = 100 \text{ mm}$; $\alpha = 60^\circ$ Variable: $D_e = 1.0B$; $1.5B$; $2.0B$
Model-2: cellular reinforcement mattress for coverage ratio (C_r) = 1.0	$CR50_{10}$ $CR50_{20}$ $CR50_{30}$	Constant: $B = 100 \text{ mm}$; $\alpha = 60^\circ$ $S_r/H = 0.2$ Variable: $D_e = 1.0B$; $1.5B$; $2.0B$ $L_r = 0.7H$ to $0.3H$
Model-3: cellular reinforcement strips for coverage ratio (C_r) = 0.5, 0.6	$CR50_{10}$ $CR50_{20}$ $CR50_{30}$	Constant: $B = 100 \text{ mm}$; $\alpha = 60^\circ$ $S_r/H = 0.2$ Variable: $D_e = 1.0B$; $1.5B$; $2.0B$ $L_r = 0.7H$ to $0.3H$

H height of slope, 500 mm, B footing width, D_e edge distance, S_r vertical spacing, L_r length of reinforcement, α slope angle

analysis were carried out for model conditions in the finite-element software (PLAXIS 3D) for fly ash slopes on rigid foundation as mentioned in Table 1. In the current study, cellular reinforcement was assigned as $CRdh$, where ‘ d ’ and ‘ h ’ are diameter and height of the unit geocell in mm (i.e., $CR50_{10}$ = cellular reinforcement of 50 mm diameter and 10 mm height).

The physical analysis of fly ash is tabulated in Table 2 as per the relevant ASTM standards. The maximum dry unit weight and optimum moisture content (OMC) of fly ash is obtained from standard Proctor tests. Fly ash has no cohesion value in the dry state, however in the presence of water while compacted it develops apparent cohesion.

As per the relevant ASTM standards the properties of reinforcement materials are tabulated in Table 3. Figure 2a represents the tensile force per unit width–strain response of a steel grid test specimen. A woven jute geotextile was placed at slope facia throughout the width along with cellular reinforcement in order to prevent escaping of fly ash from slope. Under 2-kPa normal pressure the thickness of the jute geotextile was 1.3 mm as per the relevant ASTM standards.

Table 2 Physical analysis of fly ash

Properties	Values
Dry unit weight	14.4 kN/m ³
Optimum moisture content (OMC)	18.0%
Specific gravity	2.15
Cohesion (c)	25 kPa
Angle of internal friction (ϕ)	28°
Fine sand size	16%
Silt size	78%
Clay size	6%
Liquid limit	29.54%
Plasticity	NP (non-plastic)

Figure 2b represents the tensile force per unit width–strain response of a jute geotextile specimen. The geocell used in the experimental study for validation purposes consisted of cells of 50 mm diameter (d) with varying heights (h) of 10, 20, and 30 mm made of polyethylene terephthalate (PET) plastic. Cells were interconnected by a particular type

Table 3 Properties of reinforcement materials

Reinforcement properties	Values
Steel grid reinforcement	
Tensile strength	29 kN/m
Tensile modulus	806 kN/m
Mass per unit area	264 g/m ²
Jute geotextile	
Tensile strength	10 kN/m
Tensile modulus	138 kN/m
Mass per unit area	700 g/m ²
Apparent opening size	135 μm
Plastic water bottle cell (50 mm diameter)	
Tensile strength	10 kN/m
Tensile modulus	50 kN/m

of plastic tie wires having loop tensile strength of 133 N. Fig. 2c represents the tensile force per unit width–strain response of a plastic strip specimen.

Numerical Modelling

To verify the laboratory model test results with numerical modelling, a series of three dimensional FES was carried out using PLAXIS 3D on a varying edge distance of the footing-slope system. Plaxis was chosen to validate the experimental results because, it can handle a wide range of geotechnical engineering problems mainly deep excavations, tunnels and earth structures like retaining walls, slopes, embankments, etc [50]. The intent was to create the same geometry and material conditions as in the laboratory in the 3D finite-element

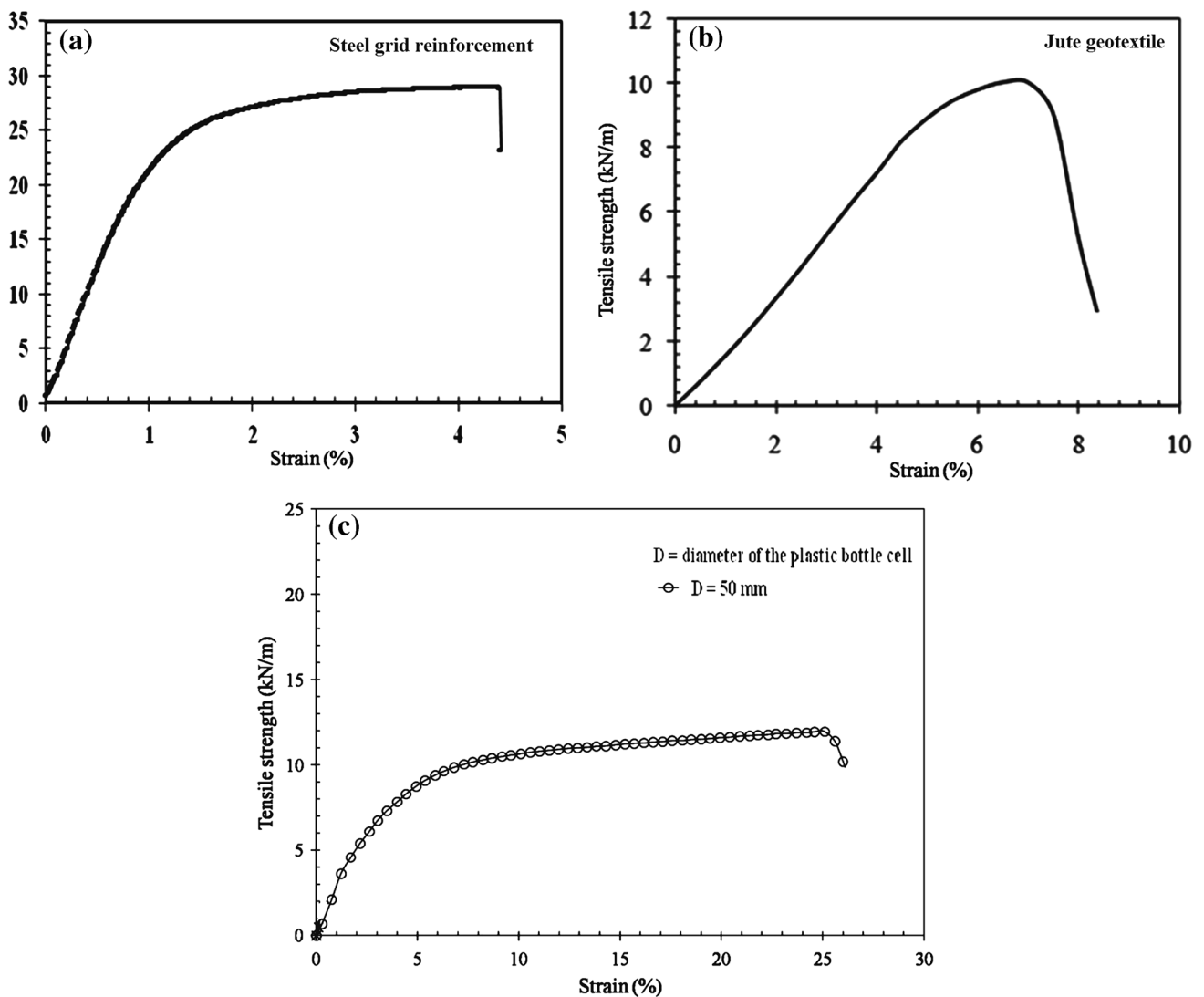


Fig. 2 Tensile force per unit width–strain responses of **a** steel grid test specimen, **b** jute geotextile specimen, **c** plastic strip specimen

modelling. Preparation of the geocell-reinforced fly ash slope in the laboratory is shown in Fig. 1b and 3D modelling of the same in the finite-element program PLAXIS 3D is shown in Fig. 3a. First, the same model geometry was created in the finite-element program over a surface area of bottom width 649 mm and top width 360 mm of the embankment, and width of slope was 500 mm to create a bottom volume of 500 mm height to represent the fly ash slope, a slope facia surface to represent steel grid-jute geotextile, interconnected circular vertical cells array to represent the cellular mattress, and a volume to represent infill fly ash.

Then the entire geometry was assigned with suitable material models and properties available in the PLAXIS 3D program so as to represent the laboratory model as perfectly as possible. The next step was mesh generation, that is, representing the entire model as an integration of many small mesh elements (connectivity plot), as shown in Fig. 3b for a mattress and strips-reinforced fly ash slope, and finally the calculation stage (plastic analysis). After conducting analyses using different types of element distributions of mesh available in PLAXIS 3D—very coarse, coarse, medium, fine, and very fine; out of all, the medium mesh distribution was optimized in the present study.

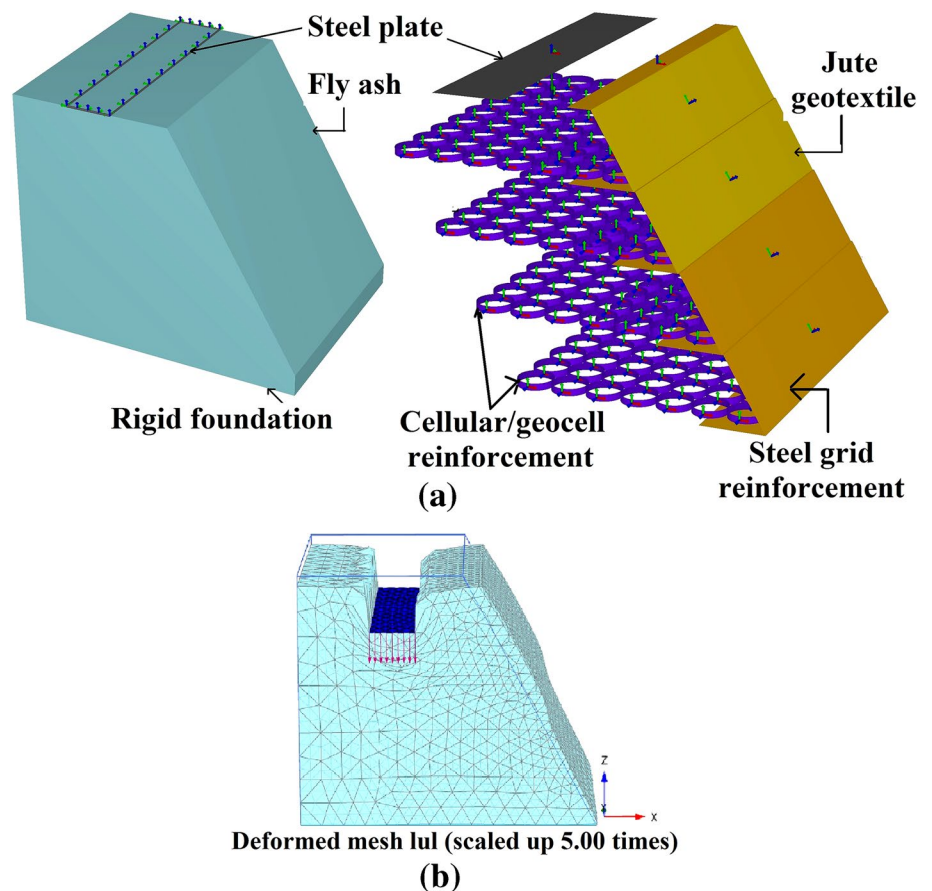
Table 4 Material properties of fly ash used in the FES

Material properties	Modeling properties
Material model	Mohr–Coulomb
Drainage type	Drained
Bulk unit weight (kN/m ³)	15.4
Cohesion (kPa)	$c' = 14$
Friction angle (°)	$\phi' = 38$
Modulus of elasticity (kPa)	$E_{50}' = 4500$
Poisson's ratio	$\nu' = 0.36$ (UR) and 0.31 (reinforced)

E' , c' , ν' , ϕ' drained parameters, UR unreinforced

The material model, drainage type, and properties of the fly ash for the finite-element modelling are reported in Table 4. To represent the basic soil elements of the 3D finite-element mesh, ten-node tetrahedral elements having three nodes at each edge of the tetrahedral were used. Numerical studies were carried out using finite element method (FEM) in order to simulate the results obtained from model studies [49].

Fig. 3 a 3D modeling of fly ash slope and geocell in finite-element program; b mesh distribution (connectivity plot) in 3D FEM for a mattress-cellular reinforced rigid bed



Material Modelling

The FEA was carried out using PLAXIS 3D software [50]. In this numerical study, the fly ash was modeled using Mohr–Coulomb model and involves five parameters; Young’s modulus (E), Poisson’s ratio (μ), cohesion(c), friction angle (Φ), and the dilatancy angle (Ψ). In addition to this, for each analysis it was necessary to specify the coefficient of earth pressure (K_0) at rest condition and bulk unit weight (γ_b) of soil. The shear stress parameters are used to describe the failure behavior of fly ash and to define these parameters series of consolidated drained (CD) triaxial tests were conducted in the laboratory. For the unreinforced case, the soil parameters adopted remain same in all the FEA. For a reinforced case, with appropriate strength reduction factors between the contact surfaces were given, and reinforcement layer was introduced at the required depth and the stiffness of reinforcement is entered as additional parameters. In this study, FEA were performed by applying zero horizontal displacements and vertical prescribed displacements to the nodes at the base of footing. The specified footing displacements were imposed in equal increments of 250 steps. The footing pressure was analyzed and calculated by dividing the ratio of resulting vertical nodal loads at the base of the footing to the width of the footing [35].

As per the relevant ASTM standards, CD triaxial tests were performed on fly ash samples prepared at OMC with dry unit weight as 87% of the maximum dry unit weight (i.e., $0.87 \times 14.4 = 12.52 \text{ kN/m}^3$) achieved during preparation of the unreinforced fly ash slopes and the reinforced fly ash slope achieved 85% of its maximum dry unit weight (i.e., $0.85 \times 14.4 = 12.24 \text{ kN/m}^3$). To simulate the laboratory test conditions the confining pressures (σ_3) 5, 10, and 15 kPa were kept low. The cohesion (c) was 25 kPa and angle of

internal friction (ϕ) of the fly ash at OMC was found to be 28° . The deviatoric stress (σ_d)–axial strain (ϵ) curves is shown in Fig. 4a. Elastic modulus of fly ash was adopted as the secant tangent modulus, E_{50}' from the deviator stress–axial strain curve at low confining pressure of 5 kPa. E_{50}' is defined as the secant modulus corresponding to 50% of the ultimate deviator stress.

The cohesion and angle of internal friction were determined from the Mohr–Coulomb failure envelope as shown in Fig. 4b and the same reported in Table 4. The same cohesion, angle of internal friction and elastic modulus were chosen for infill fly ash also for FEA because the difference was small in the achieved degree of compaction for the reinforced and unreinforced fly ash slopes. The Poisson’s ratio of the fly ash was varied in the range of 0.28–0.38 during modelling. For unreinforced fly ash, the Poisson’s ratio of 0.36 provided optimum validation with the experimental results, whereas for mattress-strips reinforced infill fly ash, it was 0.31 [46, 51].

The jute geotextile was modeled as an isotropic elastic geogrid material (available in PLAXIS 3D) having a tensile modulus of 138kN/m. The cell material was modeled as an isotropic elastic geogrid with a peak tensile modulus of 50 kN/m the same as that of the laboratory cells. Geogrids are slender structures that can only sustain tensile force and no compression, and thus they acquire only axial stiffness but no bending stiffness. After meshing, geogrids are composed of six-node triangular surface elements having three translational degrees of freedom per node with the ability to change length under tension. The interconnections of the cells were modeled using elastic anchor material (node-to-node anchor) with a tensile strength of 133 N to represent the tie wires and the anchor was a spring element. In general, the interface is weaker and more flexible than the surrounding

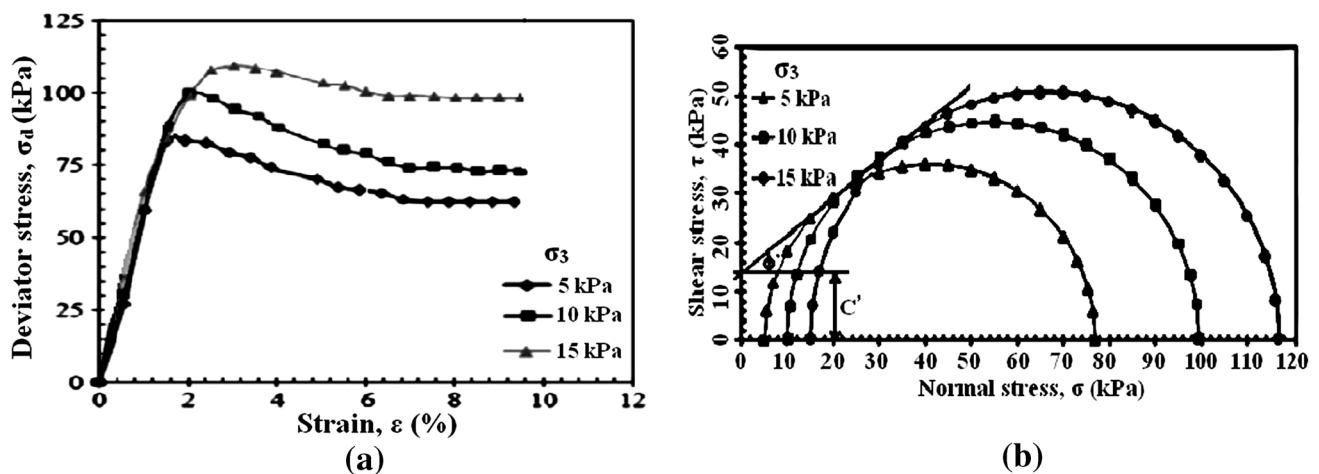


Fig. 4 a Deviatoric stress–axial strain curves at low confining pressures of 5, 10, and 15 kPa for fly ash from CD triaxial test; b Mohr–Coulomb failure envelope for fly ash

soil for real soil–structure interaction. The soil–structure interaction was simulated by adding 12-node interface elements (joint elements) to the structure. A strength reduction factor at interfaces (R_{inter}) was introduced in the modelling as available in PLAXIS 3D. The roughness of the interaction was modeled by choosing suitable values for the strength reduction factors. This factor relates the interface strength [adhesion (c_i)] and wall friction (φ_i) to the adjacent soil strength [cohesion (c_{soil})] and friction angle (φ_{soil}) as $c_i = R_{inter} \times c_{soil}$ and $\tan\varphi_i \times R_{inter} \times \tan\varphi_{soil}$. At the infill fly ash–cell wall interface, R_{inter} was assumed as 0.95, whereas at the fly ash–jute geotextile and steel grid it was assumed as 0.8. Waterman [52] suggested R_{inter} value as $R_{inter} \approx 1$ (soil/geogrid interaction) and $R_{inter} \approx 0.9$ –0.5 (soil/geotextile interaction). By using the formula $\psi \approx \phi - 30^\circ$; where the angle of dilatancy (ψ) was obtained from the friction angle (ϕ); ψ was taken as zero if the value of ϕ was $<30^\circ$ [53]. Other parameters are well defined in the PLAXIS 3D manual to perform numerical analysis.

At apex of the fly ash slope for unreinforced and cellular reinforced cases, a surface area of 100×500 mm rectangle rigid footing being pushed vertically downwards at a constant rate 2 mm/min up to 40 mm settlement. The FEA were carried out using finite element software PLAXIS 3D which enables the user to provide desirable boundary conditions. In the FEM model, the side boundaries of the embankment and fly ash bed in contact with the tank were modeled as the fly ash volume with horizontal movement restricted in the outward direction. The vertical movement was allowed along with the inward horizontal movement.

Validation of FEM Results and Discussion

General

In the FEM simulation analysis at the footing base, the average footing pressure was procured by the vertical stresses at the Gauss points in the soil elements, and the average footing settlement at the peak was procured by the vertical displacements of the nodal points. In all the cases of FEM simulations, the measured bearing capacity values were reasonably good, whereas the settlement was generally undervalue.

FEM Simulation of Unreinforced and Reinforced Fly Ash Slopes

Comparisons between the pressure–settlement responses were calculated using the FEA and the results obtained from experimental model tests for with and without reinforcements are shown in Figs. 5, 6, 7 and 8.

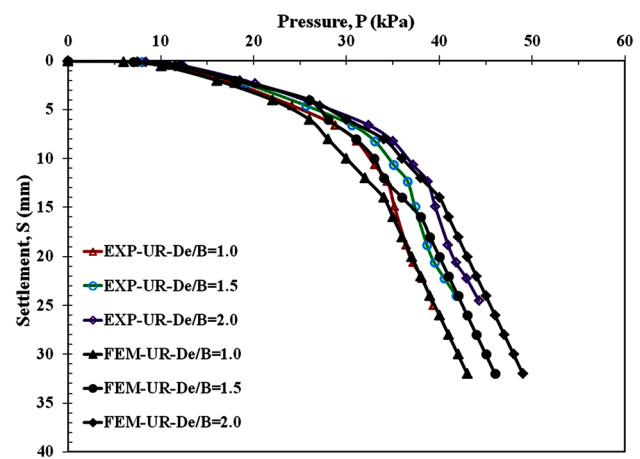


Fig. 5 Validation of the finite-element program with experimental results of pressure-settlement response of unreinforced slope

Model 1: Unreinforced Fly Ash Slope

Validation of the finite-element program with experimental results of pressure-settlement response of unreinforced slope is shown in Fig. 5. For all the unreinforced cases when the load was applied on the footing over the backfill, the slope face moved laterally causing failure and the same we can see in the FEA. Experimental results are having good agreement with FEA results. However, the impulsive trend of the footing movements towards the slope face is clearly noted for the reinforced case, while the footing tends to fail by punching on the unreinforced slope.

Model 2: Effect of Cellular Reinforced Mattress of Fly Ash Slope

Validation of the finite-element program with experimental results of footing pressure-settlement response of cellular reinforcement mattress of $D_e = 1.5B$ for $CR50_{20}$ is shown in Fig. 6. For all the (L_r/H) ratios the response of footing pressure and footing settlements was nonlinear and failure obtained from experimental studies can be quite accurately simulated with available finite element modelling analysis. The observed trend is almost found similar between footing pressure and footing settlements for both model testing and FES method. It can be seen that a reasonable agreement was found between model testing values and the FES.

Table 5 gives the comparison of improvement factor (I_f) between model testing and FES with footing settlement for different L_r/H ratios with cellular reinforcement mattress. Comparison of experimental studies and FES results reveals the maximum variations observed is about 2.70%, may be due to the dimensional assumptions in FES and the limitation of interface modelling of reinforcement. At 5 mm settlement with $CR50_{20}$ for $D_e = 1.5B$ of $L_r = 0.6H$, improved

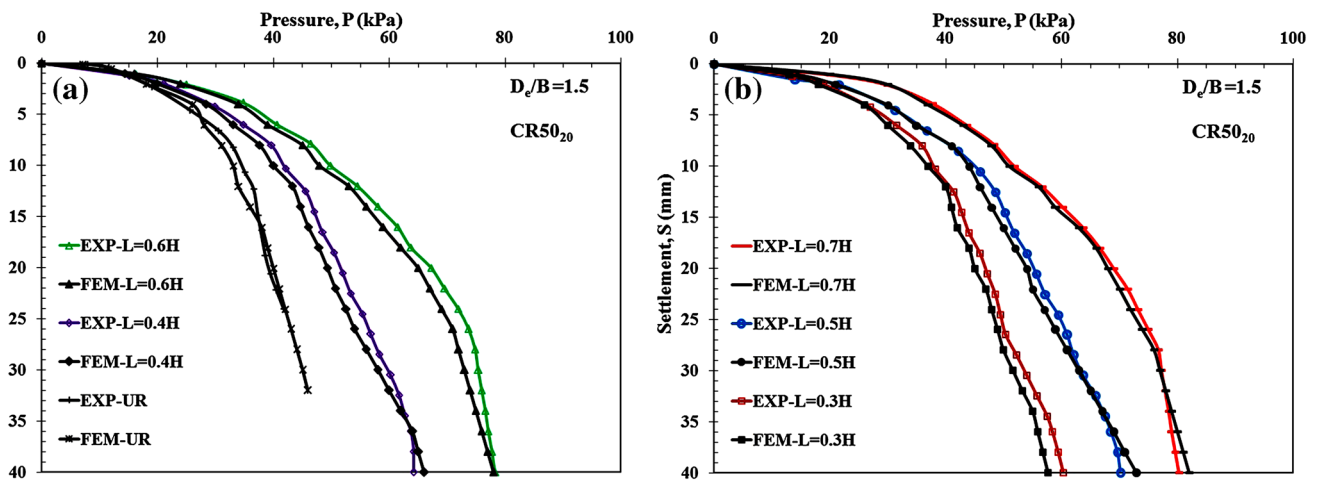


Fig. 6 Validation of the finite-element program with experimental results of pressure-settlement response of cellular reinforcement mattress of $D_e = 1.5B$ for $CR50_{20}$

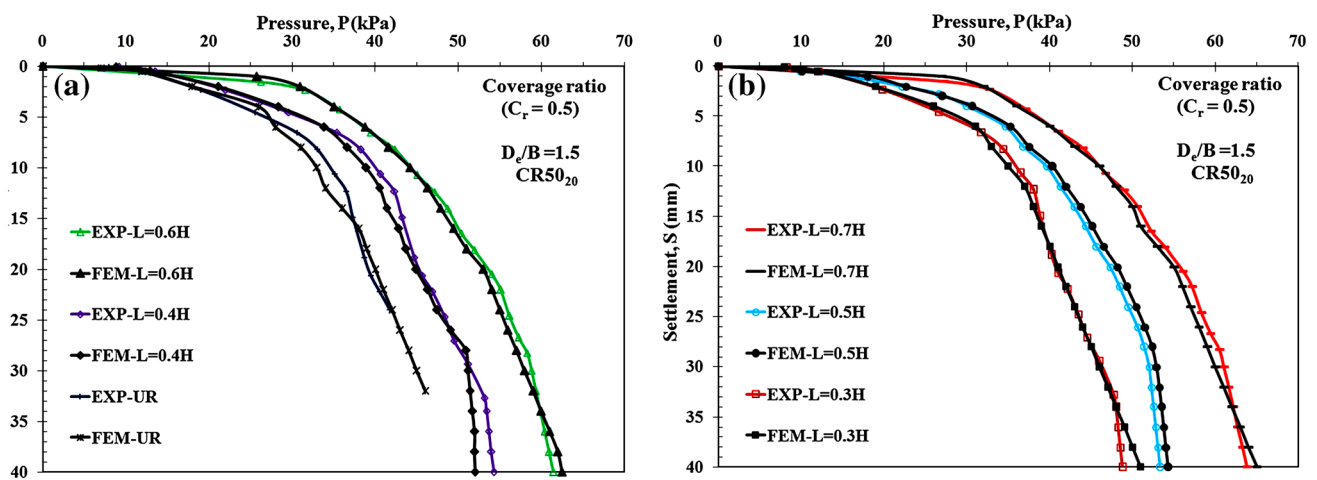


Fig. 7 Validation of the finite-element program with experimental results of pressure-settlement response of cellular reinforcement strips of $D_e = 1.5B$ ($C_r = 0.5$) for $CR50_{20}$

the pressure carrying capacity 1.89 times and 1.88 times greater the capacity of unreinforced slope for experimental and FES tests respectively, as mentioned in Table 5. With the significant increase in magnitude of (L_r/H) ratios, the backfill settlement values at failure condition got increased, however the footing pressure got increased with increase in the (L_r/H) ratios. From Fig. 6a, b we can observe that the results obtained from experimental and FES suggests that, for $CR50_{20}$ of a particular pressure were found to be nearly equal when (L_r/H) ratio was in between 0.6 and 0.7, this may be due to the slope resting on a rigid base foundation and the load is spontaneously transmitted to slopes in layers. While transferring this load, slopes with higher L_r/H ratios initially carries greater load carrying capacity because of its improved stiffness and carried higher load at failure. Significant increased

settlement values were observed when reinforcement length reduced below $0.5H$. A similar pattern was also noticed in experimental model test results. However, in average it can be seen that the results of FES are found in a reasonable agreement with the experimental study.

Model 3: Effect of Coverage Ratios of 0.5 and 0.6

The numerical simulation analysis of cellular reinforced fly ash slopes when back fill was reinforced with geocell reinforcement strips ($C_r = 0.5$ and 0.6) with varying geocell heights and (L_r/H) ratios are presented. Figures 7a, b and 8a, b show the validation of the finite-element program with experimental results of footing pressure-settlement response of cellular reinforcement strips ($C_r = 0.5$ and 0.6)

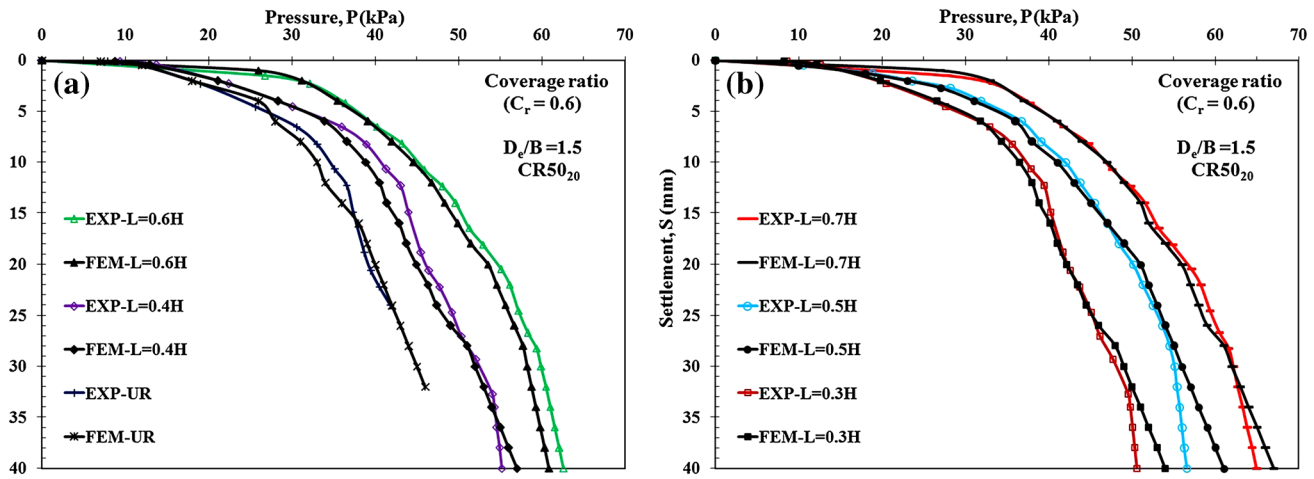


Fig. 8 Validation of the finite-element program with experimental results of pressure-settlement response of cellular reinforcement strips of $D_e = 1.5B$ ($C_r = 0.6$) for $CR50_{20}$

Table 5 Comparison of improvement factor between model testing and finite element simulation with footing settlement for different L_r/H ratios with CR mattress

Edge distance (D_e)	(CR) Dimensions mm	Improvement factor 5 mm vertical settlement								
		$L_r = 0.7H$			$L_r = 0.6H$			$L_r = 0.5H$		
		EXP	FEM	% Variations	EXP	FEM	% Variations	EXP	FEM	% Variations
1.0B	$CR50_{10}$	1.34	1.31	2.24	1.32	1.30	1.52	1.11	1.08	2.70
	$CR50_{20}$	1.52	1.50	1.32	1.50	1.49	0.67	1.36	1.35	0.74
	$CR50_{30}$	1.55	1.54	0.65	1.53	1.52	0.65	1.32	1.30	1.52
1.5B	$CR50_{10}$	1.57	1.55	1.27	1.54	1.53	0.65	1.32	1.31	0.76
	$CR50_{20}$	1.90	1.89	0.53	1.89	1.88	0.53	1.70	1.72	1.16
	$CR50_{30}$	1.91	1.90	0.52	1.90	1.91	0.52	1.70	1.71	0.58
2.0B	$CR50_{10}$	1.55	1.56	0.64	1.53	1.52	0.65	1.28	1.26	1.56
	$CR50_{20}$	1.86	1.85	0.54	1.83	1.85	1.08	1.65	1.63	1.21
	$CR50_{30}$	1.89	1.90	0.53	1.87	1.86	0.53	1.72	1.71	0.58

at $D_e = 1.5B$ for $CR50_{20}$, respectively. The footing pressure versus footing settlement responses until failure obtained from experimental studies can be quite accurately simulated with available finite element modelling analysis. The observed trend is almost found similar between footing pressure and footing settlements for both model testing and FES method. It can be seen that a reasonable agreement was found between model testing values and the finite element simulations.

Coverage Ratio, $C_r = 0.5$

Table 6 gives the comparison of improvement factor between model testing and FES with footing settlement for different L_r/H ratios with cellular reinforcement strips of $C_r = 0.5$. From Fig. 7a, b for $CR50_{20}$ when $D_e = 1.5B$ with

$L_r = 0.7$ and 0.6 gives maximum loading before failure, this is because initially load transfers to adjacent layers of embankment and gradually increases at top layers of embankment resulting in greater load-carrying capacity because of their improved stiffness. However, a maximum variation observed is about 3.33% only from experimental studies and FES results. At 5 mm settlement with $CR50_{20}$ for $D_e = 1.5B$ of $L_r = 0.6H$, improved the pressure carrying capacity 1.39 times and 1.38 times greater the capacity of unreinforced slope for experimental and FES tests respectively, as reported in Table 6.

Coverage Ratio, $C_r = 0.6$

Table 7 gives the comparison of improvement factor between model testing and FES with footing settlement for different

Table 6 Comparison of experimental studies with numerical simulation of improvement factor with footing settlement for different L_r/H ratios with strip for $C_r = 0.5$

Edge dis- tance (D_e)	(CR) Dimen- sions mm	Improvement factor 5 mm vertical settlement								
		$L_r = 0.7H$			$L_r = 0.6H$			$L_r = 0.5H$		
		EXP	FEM	% Variations	EXP	FEM	% Variations	EXP	FEM	% Variations
1.0B	CR50 ₁₀	1.13	1.11	1.77	1.11	1.09	1.80	0.90	0.87	3.33
	CR50 ₂₀	1.31	1.28	2.29	1.30	1.28	1.54	1.15	1.13	1.74
	CR50 ₃₀	1.33	1.32	0.75	1.31	1.30	0.76	1.12	1.10	1.79
1.5B	CR50 ₁₀	1.29	1.28	0.78	1.27	1.26	0.79	1.04	1.01	2.88
	CR50 ₂₀	1.41	1.40	0.71	1.39	1.38	0.72	1.20	1.21	0.83
	CR50 ₃₀	1.43	1.41	1.40	1.41	1.40	0.71	1.25	1.26	0.79
2.0B	CR50 ₁₀	1.28	1.27	0.78	1.26	1.24	1.59	1.10	1.11	0.90
	CR50 ₂₀	1.38	1.37	0.72	1.37	1.36	0.73	1.17	1.16	0.85
	CR50 ₃₀	1.41	1.42	0.70	1.39	1.38	0.72	1.24	1.23	0.81

L_r/H ratios with cellular reinforcement strips of $C_r = 0.6$. Maximum variation observed is about 2.78% only from experimental studies and FES results which is less than $C_r = 0.5$. At 5 mm settlement with CR50₂₀ for $D_e = 1.5B$ of $L_r = 0.6H$, improved the pressure carrying capacity 1.54 times and 1.53 times greater the capacity of unreinforced slope for experimental and FES tests respectively, as mentioned in Table 7. The experimental and FES results from Fig. 8a, b suggests that, CR50₂₀ and CR50₃₀ for $C_r = 0.6$, the footing settlement values for a particular footing pressure were quite similar when (L_r/H) ratio was in between 0.7 and 0.6. Reducing the (L_r/H) ratio below 0.6 showed significant increasing in the values of settlements this is because slopes with higher (L_r/H) ratios initially have greater load-carrying capacity because of the improved stiffness and more confinement effect. A similar pattern was observed in model experimental test results.

In general for cellular reinforced mattress and strips, it is also observed that with increase in length of reinforcement and cell height, the improvement in load-carrying capacity is accompanied by an increase in settlement. To form a mattress width with geocells, more numbers of cells with more connections were required, resulting in a mattress with more rigidity. Hence, the mattress had better interaction with the infill fly ash at a certain volume providing better confinement effect. Below the reinforced zone at D_e/B ratio of 1.5 for $L_r/H=0.6$ at CR50₂₀, the reinforcement enables much better load distribution over a larger area, and under higher overburden pressure more adequate anchorage resistant can be mobilized and due to this enhanced load-transfer mechanism, the tensile strength of the cellular reinforcement results in optimum utilization. Experimental and numerical findings suggested that, for all varying D_e/B ratios and geocell heights, $L_r/H=0.6$ has very close agreement with $L_r/H=0.7$

Table 7 Comparison of experimental studies with numerical simulation of improvement factor with footing settlement for different L_r/H ratios with strip for $C_r = 0.6$

Edge dis- tance (D_e)	(CR) Dimen- sions mm	Improvement factor 5 mm vertical settlement								
		$L_r = 0.7H$			$L_r = 0.6H$			$L_r = 0.5H$		
		EXP	FEM	% Variations	EXP	FEM	% Variations	EXP	FEM	% Variations
1.0B	CR50 ₁₀	1.28	1.25	2.34	1.26	1.24	1.59	1.05	1.08	2.78
	CR50 ₂₀	1.46	1.44	1.37	1.44	1.43	0.69	1.31	1.32	0.76
	CR50 ₃₀	1.48	1.47	0.68	1.46	1.47	0.68	1.17	1.19	1.68
1.5B	CR50 ₁₀	1.43	1.40	2.10	1.41	1.39	1.42	1.18	1.15	2.54
	CR50 ₂₀	1.55	1.54	0.65	1.54	1.53	0.65	1.34	1.32	1.49
	CR50 ₃₀	1.57	1.56	0.64	1.54	1.53	0.65	1.39	1.37	1.44
2.0B	CR50 ₁₀	1.41	1.40	0.71	1.39	1.37	1.44	1.24	1.22	1.61
	CR50 ₂₀	1.52	1.50	1.32	1.50	1.48	1.33	1.31	1.30	0.76
	CR50 ₃₀	1.53	1.54	0.65	1.52	1.51	0.66	1.38	1.37	0.72

for all model parameters because of increased stiffness and more confinement effect. Therefore, the improvement factor of $D_e/B = 1.5$ and 2.0 is almost same for all reinforcement lengths. Hence, from present investigation, D_e/B ratio of 1.5 at $CR50_{20}$ for $L_r/H = 0.6$ is considered as an optimized value for cellular reinforced fly ash slopes in terms of load-carrying capacity for both mattress ($C_r = 1.0$) and strips ($C_r = 0.6$) for particular fly ash and the investigated parameters.

Effect of Edge Distance of the Footing from Slope Crest in FEA

The computed results of ultimate bearing capacity (UBC) obtained from FEA is literally precise and the UBC of FEA is defined in the same way as that of experimental model tests. Figure 9 show the variations of UBC verses edge distance ratio for $CR50_{20}$ at $L_r = 0.6H$. In Fig. 9, both experimental and analytical results have been plotted for comparison. The trends shown by analytical and experimental results are having almost similar patterns. Table 8 gives the comparison of experimental studies with numerical simulation of improvement factor of UBC with edge distance

ratio for $CR50_{20}$ at $L_r = 0.6H$. Comparison of experimental studies and FES results reveals that when edge distance increases from $1B$ to $2B$, maximum to minimum percentage variation of bearing capacity was found to $6.96-0.54$. In general, with increase in edge distance from slope crest the ultimate bearing capacity of the footing increases, but in this present investigation at edge distance of $2B$, improvement factor of UBC decreases and percentage variations for both $D_e/B = 1.5$ and 2.0 for $CR50_{20}$ are almost similar. This is because from our observation during experiments and numerical modelling, the change in footing location from slope crest has dominant effect on bearing capacity criteria and also because of the passive resistance offered by fly ash slope on the reinforcements from the slope side portion and also lateral movements were decreased by inclusion of geocell reinforcement, resulting in a broader and deeper failure zone this may be one of the reason that UBC of cellular reinforcement decreases at edge distance of $2B$. The FEA results shows consistency with the experimental results and gives some assurance in the reliability of the results obtained from the model tests.

Fig. 9 Variation of ultimate bearing capacity (UBC) with edge distance ratio for $CR50_{20}$ at $L_r = 0.6H$

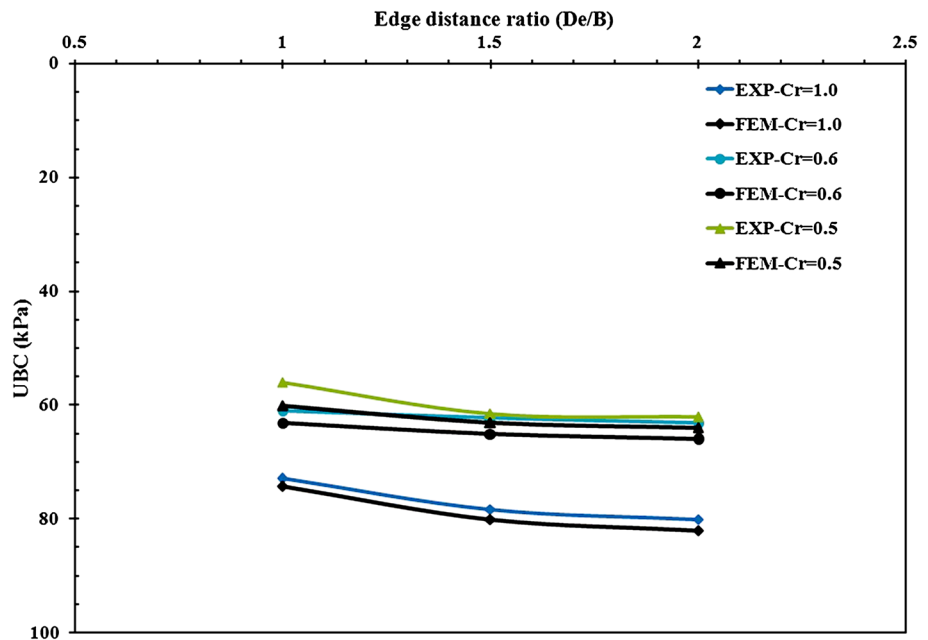


Table 8 Comparison of experimental studies with numerical simulation of improvement factor of UBC with edge distance ratio for $CR50_{20}$ at $L_r = 0.6H$

Edge distance (D_e)	Improvement factor (UBC)								
	Mattress ($C_r = 1.0$)			$C_r = 0.6$			$C_r = 0.5$		
	EXP	FEM	% Variations	EXP	FEM	% Variations	EXP	FEM	% Variations
1.0B	1.85	1.86	0.54	1.47	1.58	6.96	1.40	1.50	6.67
1.5B	1.87	1.90	1.58	1.49	1.55	3.87	1.47	1.50	2.00
2.0B	1.86	1.82	2.15	1.45	1.47	1.36	1.44	1.42	1.39

FEM Displacement Vectors and Plastic Points

For with and without reinforcement of a fly ash slope, the load-transfer mechanism can also be substantiated by the FEA results. Figures 10 and 11 presents the typical displacement vectors and plastic points obtained from the analysis for different parameters like mattress and strips for a footing on both unreinforced and reinforced slopes having $L_r/H=0.6$ and $D_e/B=1.5$ for $CR50_{20}$. Same trend can be observed for remaining modelling parameters. From the load submenu index standard fixities were selected, where a set of general boundary conditions automatically imposed to the geometry model. The boundary conditions of the finite element model were assumed such that bottom horizontal boundary was fully fixed and the vertical boundaries were free vertically

and constrained horizontally. Typical finite-element model geometry for vertical displacement is shown in Fig. 10. For all the finite-element analyses the parameters allocated for top and bottom fly ash layers were assumed to remain identical for unreinforced case. The interaction between the geocell along with steel grid-jute geotextile composite and the fly ash was modeled at both sides by means of interface elements. Suitable strength reduction factors were assigned for the reinforced system at the required depth which was introduced in the interface section. The Finite element models have the same dimensions as the experimental models. Vertical prescribed displacements were applied to carry out finite element analyses. The slopes are subjected to same amount of prescribed displacement as 50 mm. In Fig. 10 the total displacement contours shows the zone of influence

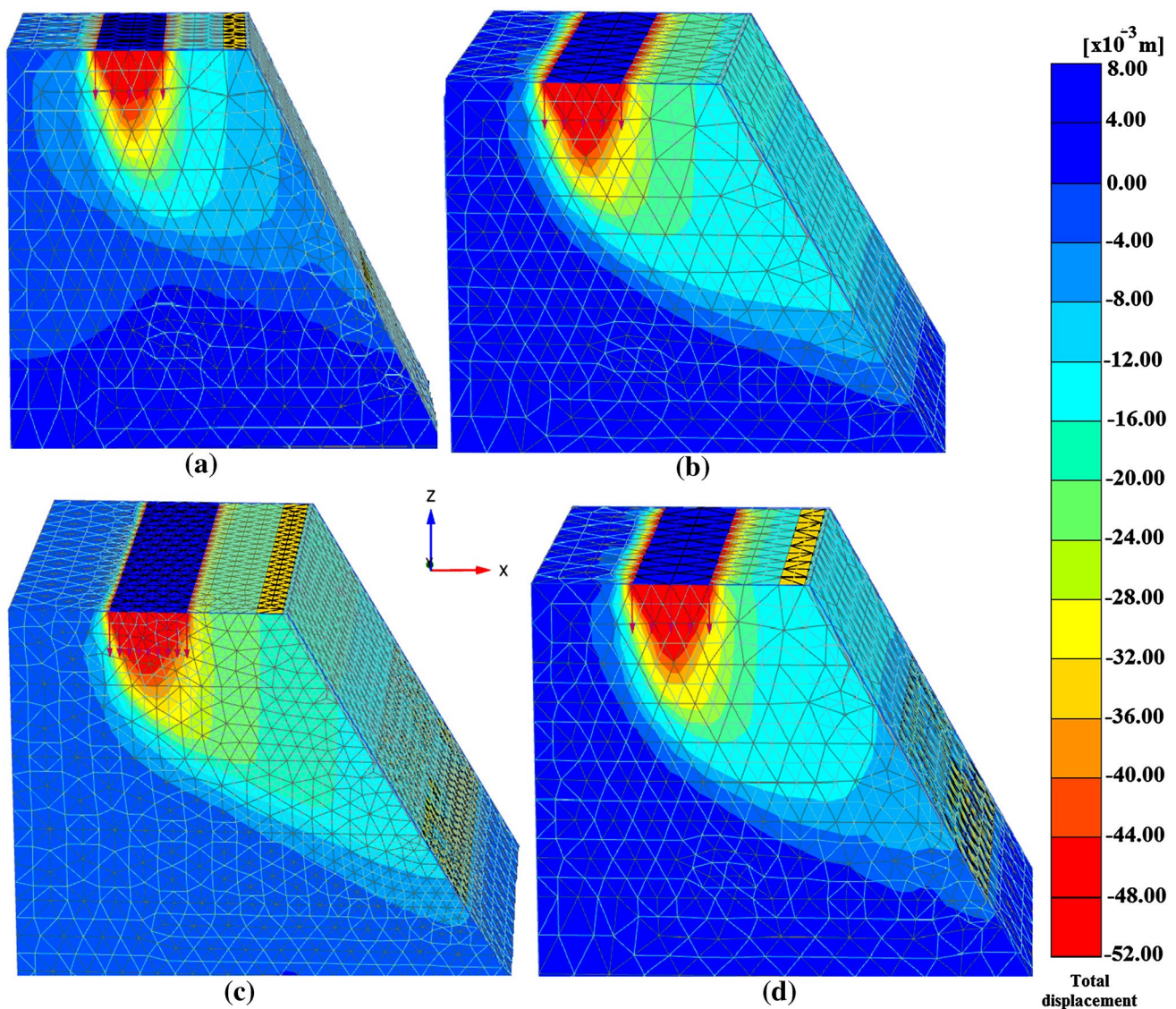


Fig. 10 Total vertical displacement (uz) of 50-mm footing settlement for $CR50_{20}$ at $D_e = 1.5B$ and $L_r = 0.6H$; **a** unreinforced; **b** cellular reinforcement mattress ($C_r = 1.0$); **c** cellular reinforcement strip ($C_r = 0.5$); **d** cellular reinforcement strip ($C_r = 0.6$)

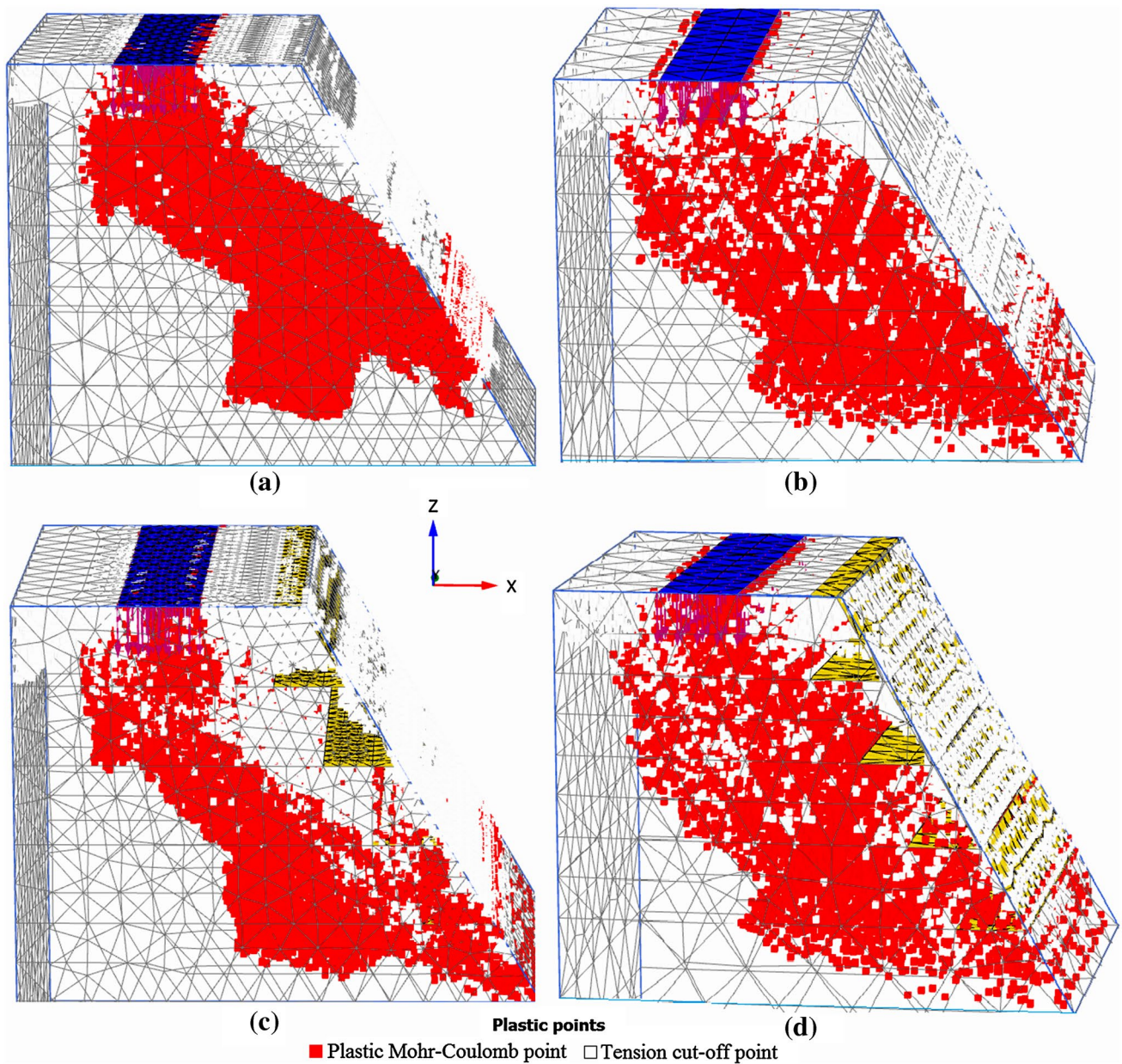


Fig. 11 Plastic points and tension cut-off points for $CR50_{20}$ at $D_e = 1.5B$ and $L_r = 0.6H$; **a** unreinforced case; **b** cellular reinforcement mattress ($C_r = 1.0$); **c** cellular reinforcement strip ($C_r = 0.5$); **d** cellular reinforcement strip ($C_r = 0.6$)

during settlement and in reinforced cases, the amount of volume influenced is more compared to that of unreinforced cases.

Figure 11 shows the plastic points and tension cut-off points generated at the edge of collapse for the footing on a rigid base. The plastic failure zone at D_e/B ratio of 1.5 when $L_r/H=0.6$ for $CR50_{20}$ of the fly ash slope is intercepted by the cellular/geocell layers and the stress distribution is extended much below reinforced zone resulting in spreading of the footing load into a wider area of a relatively rigid region of backfill material and reinforcement directly

underneath the loaded area. The overburden pressure on the geocell layer becomes inadequate when the reinforcement layer ($L_r/H=0.5-0.3$) is placed at shallow depth, resulting in anchorage resistance to the geocell against pullout force. The tension cut-off option may be used to reduce the tensile strength of a given material. In some practical problems, an area with tensile stress may develop. This indicates that filling material may fail in tension instead of in shear [50]. Tension cut-off points are concentrated at the edges of footing as well as at the slope crest as expected. The plastic zone mobilised for the footings with reinforcement in soil beneath

the footing is intercepted by geocell reinforcement layers and the zone is extended much deeper than unreinforced condition. In case of edge distance B , still the wedge is formed but it extended well below the reinforcement. Whereas for edge distance of $2B$ wedge formation below the footing is not distinct but the slope failure is conspicuously seen. Further the quantum of soil involved in failure mechanism is higher for the conditions of footing reinforcement and longer the length of reinforcement deeper is failure wedge. However, in the case of footing reinforced with longer length of reinforcement, tension cut-off points are developed at the edges of reinforcement and are dominantly in upper layers. This indicates clearly that the tension is higher in the top layers of reinforcement and they also subjected to bending.

Limitations of the Study

The Mohr–Coulomb model is a first-order model showing soil/fly ash behavior which includes only a limited number of features. This model neither includes stress path dependency or stress dependency of anisotropic stiffness or stiffness. For a fly ash slope or embankment, fly ash has a tendency to wick water into itself and it is quite possible that the lower extremities will become saturated resulting in failure of shear strength hence it is very important that the base of a fly ash embankment or slope should not be exposed to free moisture. One of the most effective ways to prevent the seepage in fly ash embankment or backfill is to place a drainage layer at the base of the embankment. No separate tests were conducted to determine the Poisson's ratio of fly ash and cellular reinforcement. However, the finite element analysis results are in reasonable agreement with experimental results.

Conclusions

The response of strip footing on unreinforced and cellular reinforced mattress-strips fly ash slopes was studied in laboratory [49]. FEA was carried out using Plaxis 3D to validate the experimental results. The important findings from the results of this investigation are presented below.

1. In FEA, the geocell material was modeled as an isotropic elastic geogrid with a peak tensile modulus of 50 kN/m the same as that of the laboratory cells. Therefore, geogrids are slender structures that can only sustain tensile force and no compression, and thus they acquire only axial stiffness but no bending stiffness.
2. In the FEA for the cellular reinforcement ($CR50_{20}$, $CR50_{30}$) of mattress and strips, the footing settlement values for a particular footing pressure were quite similar when (L_r/H) ratio was in between 0.7 and 0.6.
3. Reducing the (L_r/H) ratio below 0.6 showed significant increasing in the values of settlements; this is because slopes with higher (L_r/H) ratios initially have greater load-carrying capacity because of the improved stiffness. A similar pattern was observed in model experimental test results.
3. When edge distance increases from $1B$ to $2B$, maximum to minimum percentage variation of bearing capacity was found to be 6.96–0.54. The UBC of the footing increases with an increase in edge distance from the slope crest, but in present investigation at edge distance of $2B$, UBC decreases and percentage variations for both $D_e/B=1.5$ and 2.0 for $CR50_{20}$ are almost similar. This is because of change in footing location from slope crest has dominant effect on bearing capacity criteria and also because of the passive resistance offered by fly ash slope on the reinforcements resulting in a broader and deeper failure zone.
4. The FEM simulations with model testing findings suggested that, for all varying D_e/B ratios and geocell heights, $L_r/H=0.6$ has very close agreement with $L_r/H=0.7$ for all model parameters because of increased stiffness and more confinement effect. Therefore, the improvement factor of $D_e/B=1.5$ and 2.0 is almost same for all reinforcement lengths. Hence, from present investigation, D_e/B ratio of 1.5 at $CR50_{20}$ for $L_r/H=0.6$ is considered as an optimized value for cellular reinforced fly ash slopes in terms of load-carrying capacity for both mattress ($C_r=1.0$) and strips ($C_r=0.6$) for particular fly ash and the investigated parameters. However, further analyzes must be carried out before this can be used in actual practice.
5. Below the reinforced zone at D_e/B ratio of 1.5 for $L_r/H=0.6$ at $CR50_{20}$, the reinforcement enables much better load distribution over a larger area, and under higher overburden pressure more adequate anchorage resistant can be mobilized and due to this enhanced load-transfer mechanism, the tensile strength of the cellular reinforcement results in optimum utilization.
6. For a footing reinforced with longer length of reinforcement, tension cut-off points are developed at the edges of reinforcement and are dominantly in upper layers. This indicates clearly that the tension is higher in the top layers of reinforcement and they also subjected to bending.
7. The values obtained for all models (mattress and strips) from the numerical analysis were less when compared with experimental results. It is obvious because the field conditions cannot be simulated that exactly in the numerical analysis. The trend of the obtained curves from the numerical analysis is same as that of experimental tests.

8. Large scale model tests with large scale FEM analysis should be carried out further considering more variables are recommended in future.

References

- Kumar V, Mathur M, Sinha SS (2005) A case study: manifold increase in fly ash utilization in India. Fly ash India 2005, fly ash utilization programme (FAUP), TIFAC, DST, New Delhi, India, vol 1, pp 1.1–1.8
- Jha JN, Choudhary AK, Gill KS (2010) Stability of strip footing on reinforced fly ash slope. In: Proceedings of the 6th international congress on environmental geotechnics, New Delhi, India, November 2010, vol 2, pp 1160–1165
- Das SK, Yudhbir (2005) Geotechnical characterization of some Indian fly ashes. *J Mater Civ Eng* 17(5):544–552
- Toth PS, Chan HT, Cragg CB (1988) Coal ash as structural fill. With special reference to Ontario experience. *Can Geotech J* 25(4):644–704
- Bathurst RJ (2000) Lessons learned from full scale model tests of reinforced walls and slopes: keynote paper. In: Proceedings, 2nd Asian regional conference on geosynthetics, Kuala Lumpur, Malaysia, May 2000, vol 1, pp 1–22
- Bathurst RJ, Jones CJFP (2001) Earth retaining structures and reinforced slopes. In: Rowe R. K. (ed) *Geotechnical and geoenvironmental engineering handbook*. Springer, New York, Chap. 17
- Bathurst RJ, Blatz JA, Burger MH (2003) Performance of instrumented large-scale unreinforced and reinforced embankments loaded by a strip footing to failure. *Can Geotech J* 40(6):1067–1083
- Bathurst RJ, Hatami K, Alfaro MC, Editor SK (2012) Geosynthetic reinforced soil walls and slopes-seismic aspects. *Handbook of geosynthetic engineering*, Shukla. ICE Publishing, London, pp 317–369
- Shukla SK, Sivakugan N, Das BM (2011) A state of the art review of geosynthetic reinforced slopes. *Int J Geotech Eng* 5(1):17–32
- Choudhary AK, Verma BP (2001) Behavior of footing on reinforced sloped fill. In: Proceedings of an international conference on landmarks in earth reinforcement, Fukuoka, Kyushu Japan, November 2001, pp 535–539
- Choudhary AK, Jha JN, Gill KS (2010) Laboratory investigation of bearing capacity behavior of strip footing on reinforced fly ash slope. *Geotext Geomembr* 28(4):393–402
- Gill KS, Choudhary AK, Jha JN, Shukla SK (2011) Load bearing capacity of the footing resting on a reinforced fly ash slope. In: Proceedings of an international conference on advances in geotechnical engineering (ICAGE), Perth, Australia, November 2011, pp 531–536
- Nadaf MB, Mandal JN (2017) Model studies on fly ash slopes reinforced with planar steel grids. *Int J Geotech Eng* 11(1):20–31
- Anubhav S, Basudhar PK (2011) Numerical modelling of surface strip footing resting on double faced wrap around vertical reinforced walls. *Geosyn Int* 18(1):21–34
- El Sawwaf M (2009) Experimental and numerical study of eccentrically loaded strip footings resting on reinforced sand. *J Geotech Geoenviron Eng* 135(10):1509–1518
- Gill KS, Choudhary AK, Jha JN, Shukla SK (2012) Load bearing capacity of footing resting on the fly ash slope with multilayer reinforcements. In: Proceedings of geocongress 2012, ASCE, Oakland, CA, USA, March, 2012, pp 4262–4271
- Hatami K, Bathurst RJ (2005) Development and verification of a numerical model for the analysis of geosynthetic reinforced soil segmental walls under working stress condition. *Can Geotech J* 42(4):1066–1085
- Hatami K, Bathurst RJ (2006) A numerical model for reinforced soil segmental walls under surcharge loading. *J Geotech Geoenviron Eng ASCE* 132(6):673–684
- Muthukkumaran K, Almas Begum N (2011) Finite element analysis of laterally loaded piles on sloping ground. *Indian Geotech J* 41(3):155–161
- Balligsagar CC, Sorensen JL (1981) Fly ash as fill material. In: *Proceeding of international conference on SMFE*. Stockholm, vol 2, pp 297–301
- DiGioia AM, William LN (1972) Fly ash structural fill. *J Power Div ASCE* 98(101):77–92
- DiGioia AM Jr, McLaren RJ, Taylor LR (1979) Fly ash structural fill handbook. Electric Power Research Institute, Palo Alto. Report No. EA-1281
- Leonards GA, Baily B (1982) Pulverized coal ash as structural fill. *J Geotech Eng ASCE* 108(4):517–531
- Martin JP, Collins RA, Browning JS, Biehl FJ (1990) Properties and use of fly ashes for embankments. *J Energy Eng* 116(2):71–86
- Mir BA, Sridharan A (2013) Physical and compaction behavior of clay soil-fly ash mixtures. *Geotech Geol Eng* 31:1059–1071
- Ram Rathan Lal B, Mandal JN (2012) Feasibility study on fly ash as backfill material in cellular reinforced walls. *Electron J Geotech Eng* 17(J):1437–1458
- Ram Rathan Lal B, Mandal JN (2013) Study of cellular reinforced fly ash under triaxial loading conditions. *Int J Geotech Eng* 7(1):91–104
- Ram Rathan Lal B, Mandal JN (2014) Behavior of cellular reinforced fly-ash walls under strip loading. *J Hazard Toxic Radioact Waste Manage ASCE* 18(1):45–55
- Ram Rathan Lal B, Mandal JN (2014) Model tests on geocell walls under strip loading. *Geotech Test J* 37(3):477–487
- Indraratna B, Gasson I, Chowdhury RN (1994) Utilization of compacted coal tailings as a structural fill. *Can Geotech J* 31(10):614–623
- Lim TT, Chu J (2006) Assessment of the use of spent copper slag for land reclamation. *Waste Manage Res* 24(1):67–73
- Alamshahi S, Hataf N (2009) Bearing capacity of strip footings on sand slopes reinforced with geogrid and grid anchors. *Geotext Geomembr* 27(1):217–226
- El Sawwaf M (2007) Behaviour of strip footing on geogrid reinforced sand over a soft clay slope. *Geotext Geomembr* 25(1):50–60
- Huang C, Tatsuoka F, Sato Y (1994) Failure mechanism of reinforced sand slopes loaded with footing. *Soil Foundation* 24(2):27–40
- Lee KM, Manjunath VR (2000) Experimental and numerical studies of geosynthetic reinforced sand slopes loaded with footing. *Can Geotech J* 37(4):828–842
- Mittal S, Shah MY, Verma NK (2009) Experimental study of footing on reinforced earth slope. *Int J Geotech Eng* 3(2):251–260
- MoghaddasTafreshi SN, Dawson AR (2010) Comparison of bearing capacity of a strip footing on sand with geocell and with planar forms of geotextile reinforcement. *Geotext Geomembr* 28(1):72–84
- MoghaddasTafreshi SN, Dawson AR (2010) Behaviour of footings on reinforced sand subjected to repeated loading—comparing use of 3D and planar geotextile. *J Geotext Geomembr* 28(5):434–447
- MoghaddasTafreshi SN, Dawson AR (2012) A comparison of static and cyclic loading responses of foundations on geocell-reinforced sand. *Geotext Geomembr* 32:55–68
- Mosallanezhad NM, Hataf SH, Sadat T (2015) Experimental and large-scale field tests of grid-anchor system performance in increasing the ultimate bearing capacity of granular soils. *Can Geotech J* 53(7):1047–1058

41. Rowe RK (1987) Geotextile reinforcement on the design of low embankments on very soft weak soils. Technical report Pro 239, Ontario Ministry of Transportation and Communications, Canada
42. Selvadurai A, Gnanendran C (1989) An experimental study of a footing located on a sloped fill: influence of a soil reinforcement layer. *Can Geotech J* 26(3):467–473
43. Yoo C (2001) Laboratory investigation of bearing capacity behavior of strip footing on geogrid reinforced sand slope. *Geotext Geomembr* 19(279):298–298
44. Dutta S, Mandal JN (2016) Model studies on geocell reinforced fly ash bed overlying soft clay. *J Mater Civil Eng.* doi:[10.1061/\(ASCE\)MT.1943-5533.0001356](https://doi.org/10.1061/(ASCE)MT.1943-5533.0001356)
45. Dutta S, Mandal JN (2017) Model studies on encased fly ash column–geocell composite systems in soft clay. *J Hazard Toxic Radioact Waste Manage ASCE.* doi:[10.1061/\(ASCE\)HZ.2153-5515.0000353](https://doi.org/10.1061/(ASCE)HZ.2153-5515.0000353)
46. Gill KS, Choudhary AK, Jha JN, Shukla SK (2013) Experimental and numerical studies of loaded strip footing resting on reinforced fly ash slope. *Geosynth Int* 20(1):13–25
47. Nadaf MB, Mandal JN (2016) Steel grid reinforced fly ash slopes. In: *Proceedings of sustainability, energy, and the geoenvironment, Geo-Chicago—2016, GSP 271, ASCE, Chicago*, pp 678–687
48. Berg VE, Christopher BR, Samtani NC (2009) Design and construction of mechanically stabilized earth walls and reinforced soil slopes. Federal Highway Administration (FHWA) Technical Rep., FHWA-NHI-10-024, FHWA GEC 011, vol 1. FHWA, Washington, DC
49. Nadaf MB, Mandal JN (2017) Behavior of reinforced fly-ash slopes with cellular mattress and strips under strip loading. *J Hazard Toxic Radioact Waste (ASCE)* 21(4):04017019. doi:[http://10.1061/\(ASCE\)HZ.2153-5515.0000376](https://doi.org/http://10.1061/(ASCE)HZ.2153-5515.0000376)
50. Brinkgreve RBJ, Kumarswamy S, Swolfs WM (2016) *Plaxis 3D manual* [computer software]. Plaxis bv, Delft
51. Dutta S, Mandal JN (2016) Numerical analyses on cellular mattress reinforced fly ash beds overlying soft clay. *Int J Geomech ASCE.* doi:[10.1061/\(ASCE\)GM.1943-5622.0000772](https://doi.org/10.1061/(ASCE)GM.1943-5622.0000772)
52. Waterman D (2006) Structural elements in PLAXIS. PLAXIS finite element code for soil and rock analyses. Plaxis bv, Delft
53. Bolton MD (1986) The strength and dilatancy of sand. *Geotechnique* 36(1):65–78